Basal forebrain GABAergic innervation of olfactory bulb periglomerular interneurons

Running title: inhibitory inputs of olfactory bulb interneurons

Alvaro Sanz Diez[1], Marion Najac[2] and Didier De Saint Jan[1]

[1]Institut des Neurosciences Cellulaires et Intégratives, Centre National de la Recherche Scientifique, Unité Propre de Recherche 3212, Université de Strasbourg, 67084 Strasbourg, France, 2Department of Neurobiology, Northwestern University, Evanston, Illinois 60208.

Corresponding authors:
desaintjan@inci-cnrs.unistra.fr
Institut des Neurosciences Cellulaires et Intégratives, CNRS UPR 3212, 5 rue Blaise Pascal, 67084 Strasbourg, France

Authors contributions: ASD and DDSJ did the experiments, MN contributed essential preliminary data, DDSJ wrote the paper. All authors edited the manuscript.

Abstract: 219 words; introduction: 591 words; discussion: 1614 words

Key points summary

- Basal forebrain long-range projections to the olfactory bulb are important for olfactory sensitivity and odor discrimination.
- Using optogenetics, we confirm that basal forebrain afferents mediate IPSCs on granule and deep short axon cells. We also show that they selectively innervate specific subtypes of periglomerular (PG) cells.
- Three different subtypes of type 2 PG cells receive GABAergic IPSCs from the basal forebrain but not from other PG cells.
- Type 1 PG cells, in contrast, do not receive inputs from the basal forebrain but do receive inhibition from other PG cells.
- These results bring new light on the complexity and specificity of glomerular inhibitory circuits, as well as on their modulation by the basal forebrain.

Abstract

Olfactory bulb circuits are dominated by multiple inhibitory pathways that finely tune the activity of mitral and tufted cells, the principal neurons, and regulate odor discrimination. Granule cells mediate interglomerular lateral inhibition between mitral and tufted cells lateral dendrites whereas diverse subtypes of periglomerular (PG) cells mediate intraglomerular lateral inhibition between their apical dendrites. Deep short axon cells form broad intrabulbar inhibitory circuits that regulate both populations of interneurons. Little is known about the extrabulbar GABAergic circuits that control the activity of these various interneurons. We examined this question using patch-clamp recordings and optogenetics in olfactory bulb slices from transgenic mice. We show that axonal projections emanating from diverse basal forebrain GABAergic neurons densely project in all layers of the olfactory bulb. These long-range GABAergic projections provide a prominent synaptic input on granule and short axon cells in deep layers as well as on selective subtypes of PG cells. Specifically, three different subclasses of type 2 PG cells receive robust and target-specific basal forebrain inputs but have little local interactions with other PG cells. In contrast, type 1 PG cells are not innervated by basal forebrain fibers but do interact with other PG cells. Thus, attention-regulated basal forebrain inputs regulate inhibition in all layers of the olfactory bulb with a previously overlooked synaptic complexity that further defines interneuron subclasses.

Introduction

Olfactory bulb circuits transform the spatially organized sensory input carried by olfactory sensory neurons (OSNs) into a temporal code in mitral and tufted cells, the principal neurons that relay the information to cortical areas. In the olfactory bulb, inhibitory interneurons vastly outnumber mitral and tufted cells and form several inhibitory circuits that shape the output of principal neurons. In addition, thousands of newborn inhibitory neurons are integrated every postnatal day in the pre-existing olfactory bulb network. Inhibition thus plays fundamental roles in early olfactory processing, as demonstrated by multiple evidence *in vivo* (Abraham *et al.*, 2010;

68 Lepousez & Lledo, 2013; Fukunaga *et al.*, 2014; Gschwend *et al.*, 2015; Economo *et al.*,
69 2016).

70 Olfactory bulb interneurons are diverse but three large classes dominate: granule
71 cells, periglomerular (PG) cells and short-axon (SA) cells. Granule cells, the most
72 abundant type, form reciprocal dendrodendritic synapses with the lateral dendrites of
73 mitral and tufted cells in the external plexiform layer. PG interneurons, in contrast,
74 interact with the apical dendrites of mitral and tufted cells within the glomeruli. They
75 constitute >80% of the juxtaglomerular GABAergic cells, usually project within a single
76 glomerulus, often lack an axon and are functionally and chemically highly diverse
77 (McQuiston & Katz, 2001; Kosaka & Kosaka, 2007; Panzanelli *et al.*, 2007; Parrish-
78 Aungst *et al.*, 2007; Whitman & Greer, 2007; Kosaka & Kosaka, 2011; Najac *et al.*,
79 2015; Benito *et al.*, 2018). They have been classified in two broad functional classes
80 depending on their excitatory inputs. The majority are so-called type 2 PG cells and
81 receive excitatory inputs exclusively from the dendrites of mitral and tufted cells
82 whereas type 1 PG cells receive direct excitatory inputs from OSNs (Kosaka & Kosaka,
83 2007; Shao *et al.*, 2009). This simple synaptic classification, however, does not fully
84 reflect the functional heterogeneity of PG cells (McQuiston & Katz, 2001; Najac *et al.*,
85 2015; Benito *et al.*, 2018). Finally, SA cells with soma located in the glomerular layer
86 (superficial SA cells) or in the granule cell layer (deep or dSA cells) form broad
87 intrabulbar connections. Diverse subtypes of deep SA cells mediate a widespread
88 interneuron-specific GABAergic inhibition (Eyre *et al.*, 2008; Boyd *et al.*, 2012; Burton
89 *et al.*, 2017) whereas superficial SA cells are tyrosine hydroxylase (TH)-expressing
90 mixed dopaminergic/GABAergic neurons that regulate glutamate release from OSNs
91 and monosynaptically inhibit external tufted cells (Liu *et al.*, 2013; Whitesell *et al.*,
92 2013).

93 Granule, PG and SA cells receive GABAergic synaptic inputs but only a few studies
94 have investigated their origin. These inputs could arise from local intrabulbar
95 interactions or from extrabulbar afferences. The olfactory bulb receives centrifugal
96 GABAergic projections from the basal forebrain, particularly from the horizontal limb
97 of the Diagonal Band of Broca (HDB) and from the magnocellular preoptic nucleus
98 (MCPO) (Zaborszky *et al.*, 1986; Gracia-Llanes *et al.*, 2010; Niedworok *et al.*, 2012).
99 These long-range projections make functional connections with granule (Nunez-Parra

100 *et al.*, 2013) and dSA cells (Case *et al.*, 2017) and their pharmacological inactivation
101 impairs olfactory sensitivity (Nunez-Parra *et al.*, 2013). Little is known, however, about
102 their connections in the glomerular layer. We here examined the targets of centrifugal
103 basal forebrain axons in olfactory bulb interneurons. We used patch-clamp recording
104 and light activation of channelrhodopsin-2 (ChR2) targeted to basal forebrain
105 GABAergic neurons in acute slices from dlx5/6-Cre transgenic mice. We specifically
106 focused on PG cells and examined whether GABAergic inputs differ in distinct
107 subclasses of PG cells. The results indicate that long-range basal forebrain GABAergic
108 projections broadly regulate olfactory bulb circuits and innervate specific PG cell
109 subtypes with a previously unexpected level of synaptic complexity.
110

111 **Materials and Methods**

112 *Animals*. All experimental procedures were approved by the French Ministry and the
113 local ethic committee for animal experimentation (C.R.E.M.E.A.S). We used dlx5/6-Cre
114 female mice that express the Cre recombinase under the control of the regulatory
115 sequences of the dlx5 and dlx6 genes (Monory *et al.*, 2006), and Kv3.1-EYFP mice of
116 either sex that express the enhanced yellow fluorescent protein (EYFP) under the
117 control of the Kv3.1 K^+ channel promoter (Metzger *et al.*, 2002).

118 *Slice preparation.* 3 weeks to 3 month-old mice were killed by decapitation and the
119 olfactory bulbs rapidly removed in ice-cold oxygenated (95% O2-5% CO2) solution
120 containing (in mM): 83 NaCl, 26.2 NaHCO3, 1 NaH2PO4, 2.5 KCl, 3.3 MgSO4, 0.5 CaCl2,
121 70 sucrose and 22 D-glucose (pH 7.3, osmolarity 300 mOsm/l). Horizontal olfactory
122 bulb slices (300 µm) were cut using a Microm HM 650V vibratome (Microm, Germany)
123 in the same solution; incubated for 30-40 minutes at 34°C; stored at room
124 temperature in a regular artificial cerebrospinal fluid (ACSF) until use. ACSF contained
125 (in mM): 125 NaCl, 25 NaHCO3, 2.5 KCl, 1.25 NaH2PO4, 1 MgCl2, 2 CaCl2 and 25 D-
126 glucose and was continuously bubbled with 95% O2-5% CO2.

127 *Electrophysiological recordings.* Experiments were conducted at 32-34°C under an
128 upright microscope (SliceScope, Scientifica, Uckfield, UK) with differential interference
129 contrast (DIC) optics. Whole-cell recordings were made with glass pipettes (3-6 MΩ)
130 filled with a K-gluconate-based internal solution containing (in mM): 135 K-gluconate,
131 2 $MgCl_2$, 0.025 $CaCl_2$, 1 EGTA, 4 Na-ATP, 0.5 Na-GTP, 10 Hepes (pH 7.3, 280 mOsm).

132 Atto 594 (10 µM, Sigma) was added to the internal solution in order to visualize the
133 cell morphology during the recording. Loose cell-attached recordings (15-100 MΩ seal
134 resistance) were made with pipettes filled with ACSF. Olfactory nerves (ON) projecting
135 inside a given glomerulus were electrically stimulated using a theta pipette filled with
136 ACSF as previously described (Najac *et al.*, 2015). The electrical stimulus (100 µs) was
137 delivered using a Digitimer DS3 (Digitimer, Welwyn Garden City, UK). Optical
138 stimulation was done through a blue (490 nm) CoolLED pE 100 (CoolLED Ltd., Andover,
139 UK) directed through the 40X objective of the microscope.
140 *Cell selection.* Visual online inspection of dye-filled neurons combined with functional
141 properties were used to select the cells included in our analysis. Morphology was
142 assessed during recording upon visual inspection of dye-filled cells. PG cells were
143 selected based on the small size (5-7 µm) of their cell body, their position close to the
144 edge of the glomerulus and their small dendritic tree that ramified in a single
145 glomerulus. Superficial SA cells, with larger cell bodies and processes that broadly
146 ramified between or within several glomeruli were excluded from the analysis. PG cell
147 morphology was not reconstructed post-hoc because pipette withdraw after recording
148 inevitably damaged these cells. Deep SA cells were most often found within the IPL,
149 sometimes within the granule cell layer and selected based upon their cell body that
150 was larger (>10 µm) than granule cells' soma. Moreover, many had a spontaneous
151 high-frequency firing in the cell-attached mode (Eyre *et al.*, 2008). Cell morphology
152 was reconstructed in a subset of dSA and granule cells. To do so, neurobiotin (Vector
153 Laboratories INC., Burlingame, CA) was added to the intracellular solution (1mg/ml).
154 The patch pipette was slowly withdrawn after the recording to avoid damaging the cell
155 body. The slice was then fixed in 4% paraformaldehyde overnight, washed 3 times with
156 PBS and incubated in a permeabilizing solution containing Cy-5 conjugated streptavidin
157 (1 µg/ml; Thermo Fischer Scientific, Waltham, MA) overnight. After 3 rinses with PBS,
158 sections were mounted. Labeled cells were imaged with a confocal microscope (Leica
159 TCS SP5, Leica Microsystems, Wetzlar, Germany).

160 Recordings were acquired with a multiclamp 700B amplifier (Molecular Devices,
161 Sunnyvale, CA), low-passed filtered at 2-4 kHz and digitized at 10 kHz using the
162 AxoGraph X software (Axograph Scientific). In current-clamp recordings, a constant

163 hyperpolarizing current was injected in order to maintain the cell at a potential of -60/-
164 70 mV. In voltage-clamp recordings, access resistance (Ra<30 MΩ for PG, granule and
165 deep SA cells) was not compensated. Voltages indicated in the paper were corrected
166 for the junction potential (-15 mV).
167 *Drugs.* 6-nitro-7-sulfamoylbenzo[f]quinoxaline-2,3-dione (NBQX), D-2-Amino-5-
168 phosphonopentanoic acid (D-AP5), 2-(3-carboxypropyl)-3-amino-6-(4
169 methoxyphenyl)pyridazinium bromide (GBZ), mecamylamine hydrochloride (MECA)
170 and atropine were purchased from Abcam Biochemicals.
171 *Stereotaxic viral injections*. 3-6 weeks old dlx5/6-cre female mice were anesthetized
172 with intraperitoneal injection of ketamine (20%), acepromazine (6%) and
173 medetomidine (11.8%) mix (100µl/10g) and placed in a stereotaxic apparatus. Mice
174 were craneotomized and a volume of 200-500 nl of
175 AAV9.EF1a.DIO.hChR2(H134R).eYFP.WPRE.hGH or AAV9.EF1a.DIO.eYFP.WPRE.hGH
176 (University of Pennsylvania Viral Vector Core) was stereotaxically injected with a
177 Pneumatic Picopump PV 820, at 0.2 mm AP, -1.6 mm ML and -5.6 mm DV from
178 bregma. After surgery, mice were injected with Metacam 100 (meloxicam) (5%)
179 (100µl/10g), Antisedan (atipamezol) (2.5%) (100µl/10g), rehydrated with 1 ml of NaCl
180 0.9% and placed under a heating lamp. Mice recovered during 3-4 weeks after
181 injection before anatomical or physiological experiments.
182 *Analysis.* EPSCs, IPSCs or photocurrent amplitudes were measured as the peak of an
183 average response computed from multiple sweeps. The decay of light-evoked IPSCs
184 was most often best fitted with a double exponential with time t=0 at the peak of the
185 current. Time constant values indicated in the text are weighted decay time constants
186 calculated using the following equation: $\tau_w = (\tau_1 A_1 + \tau_2 A_2)/(A_1 + A_2)$ where τ_1 and τ_2 are
187 the fast and slow decay time constants and A_1 and A_2 are the equivalent amplitude
188 weighting factors. The onset of EPSCs and IPSCs was measured at 5% of the first peak
189 of the response. The latency of an ON-evoked EPSC was defined as the time interval
190 between the beginning of the stimulation artifact and the onset of the EPSC. The
191 latency of a light-evoked IPSC was defined as the time interval between the onset of
192 light and the onset of IPSC. The jitter of evoked EPSCs and IPSCs was defined as the
193 standard deviation (SD) of their latencies. To estimate the duration of an ON-evoked
194 plurisynaptic excitatory response, individual EPSCs with amplitude >5 pA were

automatically detected by the Axograph X software using a sliding template function. PSTH (peri stimulus time histograms) representing the cumulative number of EPSCs per 20 ms bin across several consecutive sweeps were constructed. We then determined the time needed after stimulation for the EPSC frequency to come back to baseline frequency + 2 SD during at least five consecutive bins. Baseline frequency was calculated over the 25 bins (i.e. 500 ms) preceding the stimulation.

Statistics. Data are expressed as mean ± SD unless otherwise indicated in the text. We used the Student's *t*-test to assess the statistical difference between paired sets of data with normal distribution, the non-parametric Wilcoxon-Mann-Whitney rank sum test to assess the statistical difference between unpaired sets of data, the Kruskal-Wallis test for data sets with more than two variables and p-values are reported.

Immunohistochemistry. Adult mice (1-3 months) were deeply anesthetized with intraperitoneal injection of xylazine (6.3%) and ketamine (25%) and intracardially perfused with 4% paraformaldehyde (PFA). Brains were removed and kept in 4% PFA overnight. Slices were cut (50 µm thick) with a vibratome (Leica VT 1000S). Blocking steps were performed using a PBS solution containing 2% BSA or 5% goat serum and 0.3% Triton X-100 during 2h. Sections were incubated overnight at 4°C with primary antibodies: goat anti-choline acetyltransferase (ChAT; 1:500; Millipore Cat# AB144P, RRID:AB_2079751), mouse anti-parvalbumin (PV; 1:1000; Sigma-Aldrich Cat# P3088, RRID:AB_477329), rabbit anti-calretinin (CR; 1:1000; Swant Cat# 7697, RRID:AB_2721226) or mouse anti-calbindin D28K (CB; 1:1000; Sigma-Aldrich Cat# C9848, RRID:AB_476894). After three washes in PBS, sections were incubated 2 hours at room temperature with the corresponding secondary antibodies —Alexa fluor 633 conjugated goat anti-rabbit (1:500; ThermoFisher A-21070) and Alexa fluor 633 conjugated goat anti-mouse (1:500; ThermoFisher A-21050) or Alexa fluor 647 conjugated donkey anti-goat (1:200; ThermoFisher A-21447). After three washes, sections were mounted in Prolong Diamond Antifade Mountant (ThermoFisher). Images were taken using a Leica TCS SP5 II confocal microscope or an Axio Imager M2 for mosaic images. Immunostained and EYFP-expressing cells were manually counted using Cell counter plug-in on Fiji software.

227

228

229 **Results**

230 **Selective expression of ChR2 in GABAergic neurons of the basal forebrain**

231 We used an optogenetic approach to map the functional synaptic connections of
232 basal forebrain GABAergic neurons onto olfactory bulb interneurons. We injected an
233 adeno-associated virus encoding a Cre-inducible ChR2-EYFP fusion protein in the basal
234 forebrain of dlx5/6-Cre mice, a transgenic line that expresses the Cre recombinase
235 exclusively in GABAergic neurons in the forebrain (Monory *et al.*, 2006)(Figure 1A).
236 These injections produced a dense EYFP labeling of fibers in the olfactory bulb. Labeled
237 fibers were particularly abundant in the granule cell layer and in the glomerular layer
238 of the bulb, similarly to a previous study using a Cre-dependent viral approach in the
239 GAD65-Cre mouse (Nunez-Parra *et al.*, 2013). In the basal forebrain, expression of
240 ChR2-EYFP was intense around the injection site but was limited to the membrane,
241 making cell bodies difficult to distinguish. Hence, we injected the same virus expressing
242 cytosolic EYFP to verify the specificity of the recombination in GABAergic neurons
243 (Figure 1B, n=5 mice). EYFP was expressed in cell bodies of various sizes around the
244 injection site. Some of these cells also expressed the calcium-binding proteins
245 calretinin (CR, n=122 cells counted), calbindin (CB, n=54) or parvalbumin (PV, n=25),
246 three classical markers of GABAergic neurons that label non-overlapping neural
247 populations in the basal forebrain (Zaborszky *et al.*, 2005). EYFP also colocalized with
248 choline acetyltransferase (ChAT), the enzyme for acetylcholine synthesis, in about 1/3
249 of the ChAT(+) neurons counted (n=63/190 cells), consistent with the idea that
250 cholinergic neurons in the basal forebrain are also GABAergic (Saunders *et al.*, 2015).

251

252 **Synaptic connections of basal forebrain axons in the olfactory bulb**

253 We then tested the synaptic connections made by ChR2-expressing basal
254 forebrain axons in the olfactory bulb using whole-cell voltage-clamp recordings in
255 olfactory bulb slices. Consistent with previous reports (Nunez-Parra *et al.*, 2013; Case
256 *et al.*, 2017), activating ChR2-expressing basal forebrain axons with brief (1-10 ms)
257 flashes of blue light evoked outward inhibitory postsynaptic currents (IPSCs) in dSA
258 cells (n=11/11, range 30-681 pA, mean 368±166 pA at Vh between -15 and -35 mV,

259 Figure 2A) and in granule cells (n=10/12, range 31-464 pA, mean 148±124 pA at Vh=0
260 mV, Figure 2B). Light-evoked IPSCs had fast onset latencies (dSA: 1.6±0.35 ms, granule:
261 2.2±0.78 ms) and little jitter (dSA: 125±160 µs, granule: 274±170 µs), consistent with
262 monosynaptic transmission. In 3 of the 11 dSA cells tested, the response had two
263 components that reversed at different potentials. At Vh=-70 mV, the response was
264 biphasic with an outward component that was blocked by the $GABA_A$ receptor
265 antagonist gabazine (GBZ, 5 µM), and an inward component that persisted in the
266 presence of GBZ but was inhibited by the nicotinic receptor antagonist mecamylamine
267 (MECA, 20 µM)(not shown). These dual responses are similar to those mediated by
268 basal forebrain neurons that release both GABA and acetylcholine onto a specific
269 subtype of dSA cells (Case et al. 2017) and were therefore not further studied.

270 Most PG cells tested also responded to the photostimulation with an IPSC
271 (n=73/94, range 6-974 pA, mean 231±218 pA at Vh=0 mV)(Figure 2C). In the majority
272 of cells, light-evoked IPSCs had a short (<2 ms) onset latency that varied little across
273 sweeps (jitter <200 µs), consistent with monosynaptic inputs (Figure 2E). However, in
274 some cells, as in the case illustrated in Figure 2C, evoked IPSCs had longer and more
275 variable onset latencies, displayed multiple peaks and had deflections during the rising
276 phase. These complex responses resulting from summating asynchronous IPSCs could
277 reflect spike asynchrony in presynaptic axons of different lengths. They could also arise
278 from a multisynaptic pathway wherein light activation of the basal forebrain
279 cholinergic afferents directly activate juxtaglomerular GABAergic neurons innervating
280 PG cells or, indirectly, via the activation of mitral and tufted cells (Liu *et al.*, 2015). To
281 test this possibility, we blocked the glutamatergic transmission with the AMPA and
282 NMDA receptor antagonists NBQX and D-AP5, respectively (n=14 PG cells), the
283 cholinergic transmission with the nicotinic and muscarinic ACh receptor antagonists
284 mecamylamine and atropine, respectively (n=6), or both pathways with a cocktail of
285 these four drugs (n=4). These blockers had no effect on light-evoked IPSCs, even on
286 complex ones (Figure 2C). Hence, our results are consistent with direct monosynaptic
287 inputs of basal forebrain axons onto PG cells and confirm previous morphological
288 evidence (Gracia-Llanes *et al.*, 2010).

289 Evoked IPSCs recorded in ACSF or in the presence of acetylcholine and glutamate
290 receptor blockers were then pooled for analysis. They were totally abolished by GBZ

291 (n=11 PG cells, Figure 2C) and reversed at the expected equilibrium potential for
292 chloride (ECl=-88 mV in our recording conditions, n=12 PG cells, Figure 2D). Light-
293 evoked IPSCs had a uniformly fast time course in dSA cells (mean decay time constant
294 11.4±5.7 ms) and in granule cells (29±6.3 ms). In contrast, the duration of light-evoked
295 IPSCs was highly variable in PG cells (decay time constant range 6-254 ms, mean
296 48.7±57.0 ms)(Figure 2F). However, light-responsive PG cells had diverse firing and
297 synaptic properties, suggesting that the variable time course of their basal forebrain
298 input may reflect PG cell diversity. To further validate this possibility, we classified the
299 recorded PG cells in distinct subtypes based on their membrane properties, ON-evoked
300 synaptic responses and light-evoked GABAergic synaptic inputs.
301
302 **Type 1 PG cells are not innervated by basal forebrain afferents**
303 Type 1 PG cells constituted ~10% of the PG cells recorded in dlx5/6;ChR2-EYFP mice
304 (n=9 cells). These neurons fired multiple action potentials in response to a membrane
305 supra-threshold step depolarization. Their discharge was regular (n=2), irregular (as in
306 Figure 3A, n=3) or a burst of spikes (n=3). They responded to the electrical stimulation
307 of OSN axons with a fast onset monosynaptic EPSC (mean latency 1.59±0.25 ms)(Figure
308 3B and 3E). The onset of this EPSC varied little across trials even at low intensities of
309 stimulation (jitter 90±40 µs) whereas the response of type 2 PG cells had a longer
310 onset latency (>2 ms) that increased and became more variable with stimulations of
311 lower intensity (Figure 3E), as previously shown (Shao *et al.*, 2009; Najac *et al.*, 2015).
312 ON stimulation also induced IPSCs in 8/9 type 1 PG cells voltage-clamped at Vh=0 mV,
313 i.e. around the reversal potential for excitation (Figure 3B, 3D). This inhibitory response
314 was composed of multiple asynchronous IPSCs, consistent with a plurisynaptic input
315 generated within the glomerular network by other PG cells activated by the
316 stimulation. However, none of the 9 type 1 PG cells tested responded to the photo
317 stimulation of the basal forebrain fibers (Figure 3C). Thus, type 1 PG cells receive
318 inhibitory inputs from neighboring PG cells but not from the basal forebrain.
319
320 **Different classes of type 2 PG cells receive basal forebrain inputs with target-specific**
321 **properties**

322 Type 2 PG cells were largely predominant in our recordings in dlx5/6;ChR2-EYFP mice
323 (n=68) and all PG cells responding to the flash of blue light with an IPSC were type 2 PG
324 cells. We classified these type 2 PG cells in three subclasses, based on their membrane
325 properties, ON-evoked synaptic responses and light-evoked basal forebrain inputs, as
326 followed:
327
328 **1. CR-expressing type 2 PG cells**
329 The most numerous cell type (n=29) showed the distinctive immature-like membrane
330 and synaptic properties of CR-expressing PG cells (Fogli Iseppe *et al.*, 2016; Benito *et*
331 *al.*, 2018), consistent with the predominance of this subtype within the entire
332 population. These cells fired at most a single action potential or a spikelet and were
333 passively depolarized by a suprathreshold current step (Figure 4A). In addition, these
334 PG cells received few spontaneous EPSCs (not shown), had small ON-evoked excitatory
335 inputs (Figure 4B, 4C) and, usually, a large electrical membrane resistance (Figure 4D).
336 ON stimulations evoked small IPSCs or no IPSC at all in these cells clamped at Vh=0mV
337 (Figure 4B, 4C) as we previously reported in genetically-identified CR-expressing PG
338 cells (Benito *et al.*, 2018). In contrast, photo stimulation of basal forebrain fibers
339 evoked a GBZ-sensitive IPSC in 27/29 cells (Figure 4E). These light-evoked IPSCs were
340 often large (average amplitude 294±196 pA, range 6-741 pA) and always fast (average
341 decay time constant 11.9±3.6 ms, range 6-21 ms)(Figure 4E). Thus, a fast basal
342 forebrain-mediated GABAergic input is another attribute of CR-expressing PG cells.
343
344 **2. CB-like type 2 PG cells with short ON-evoked excitatory responses**
345 The second group of type 2 PG cells (n=17) included cells that responded to ON
346 stimulations with a short burst of asynchronous EPSCs that lasted only few tens of ms
347 (average duration 41±27 ms)(Figure 5B). We have previously shown that this kind of
348 response is observed in a heterogeneous subclass of PG cells that includes CB-
349 expressing PG cells (Najac *et al.*, 2015). Cells classified in this group were thus called
350 CB-like PG cells. Their ON-evoked response is surprisingly much shorter than the firing
351 of the presynaptic mitral and tufted cells, independent of the stimulation strength.
352 However, the mechanism that limits glutamate release on these PG cells is still
353 unknown. In the present study, the majority (n=9) responded to a depolarizing current

354 step with a single spike preceding a plateau potential. However, some cells had a
355 regular firing (n=3) and others responded with action potentials riding on a calcium
356 spike (n=3). Photo stimulation of basal forebrain fibers evoked an IPSC in 12 of these
357 17 CB-like cells (Figure 5D). Light-evoked responses had a mean amplitude of 129±96
358 pA (range 24-324 pA) and a decay time constant ranging from 6.7 to 53.8 ms (mean
359 26±14 ms)(Figure 5D), significantly slower than in CR-like PG cells (p=0.0060, Wilcoxon
360 test). In contrast, ON stimulation did not evoke IPSCs (Figure 5B, 5C), suggesting that
361 these cells are not connected to other PG cells.
362 To confirm the absence of connections with other PG cells, we used the Kv3.1-EYFP
363 reporter mouse. A population of type 2 PG cells with short ON-evoked responses is
364 labeled in this mouse, including CB-expressing cells (Najac *et al.*, 2015). In these
365 experiments, we recorded the whole-cell voltage-clamp response of EYFP(+) PG cells
366 while simultaneously monitoring in loose cell-attached the discharge of a control PG
367 cell projecting into the same glomerulus (either EYFP(+), n=4, or EYFP(-), n=5, Figure
368 5F). ON stimulations that efficiently drove the firing of the control PG cell induced a
369 robust excitatory response in EYFP(+) PG cells clamped at Vh=-75 mV. This stimulation,
370 however, did not evoke any IPSC when cells were clamped at Vh=0mV (n=9). In a
371 subset of experiments, increasing the stimulation intensity by a factor of 10 also failed
372 to evoke IPSCs (n=6). In contrast, an electrical stimulation in the glomerular layer at
373 >200 µm away from the recorded PG cell evoked a reliable GBZ-sensitive IPSC in
374 EYFP(+) PG cells (n=16, average amplitude 87±48 pA at Vh=0 mV; decay time constant:
375 30±13 ms, range 7.7-53.6 ms) that persisted in the presence of NBQX and D-AP5 (not
376 shown). Our results suggest that this IPSC is mediated by basal forebrain axons
377 ramifying in the glomerular layer, although the possibility that dSA cells also innervate
378 these PG cells cannot be excluded. Thus, CB-like type 2 PG cells responding to the
379 stimulation of the olfactory nerve with a short excitatory response do not interact
380 locally with other PG cells but do receive a prominent GABAergic input from the basal
381 forebrain.
382
383 **3. Type 2 PG cells with long-lasting ON-evoked excitatory responses**
384 The third group of type 2 PG cells (n=18) does not correspond to any known
385 genetically-identified PG cell subtype described so far. It is composed of cells that all

386 responded to the injection of a depolarizing step with a regular firing (Figure 6A). On
387 average, these cells fired up to 27±6 action potentials during a 500 ms-long
388 suprathreshold step, a high frequency that distinguishes them from small TH(+)
389 juxtaglomerular cells that fire at a lower rate (Galliano *et al.*, 2018). In addition, they
390 responded to the ON stimulation with a long-lasting barrage of EPSCs, often lasting
391 several hundreds of milliseconds (average 1050±610 ms)(Figure 6B). These long
392 responses also contrast with the short burst of EPSCs evoked in TH(+) juxtaglomerular
393 cells (Kiyokage *et al.*, 2010) but match well with the prolonged ON-evoked firing in
394 mitral and tufted cells (Najac *et al.*, 2015; Geramita & Urban, 2017). Moreover, 17/18
395 cells in this group responded to the photo stimulation of the basal forebrain axons
396 with a prolonged IPSC (IPSC amplitude 193±247 pA, range 11-850 pA; average decay
397 time constant 116±63 ms, range 40-254 ms, $p<0.0001$ for comparison with both CR-
398 like and CB-like PG cells, Wilcoxon test)(Figure 6D). These basal forebrain-mediated
399 IPSCs were much larger than the ON-evoked IPSCs that were eventually observed in
400 6/11 PG cells (Figure 6C). Thus, long-lasting basal forebrain-mediated IPSCs are found
401 in a specific and homogeneous subclass of regularly firing PG cells that responds to an
402 ON input with a remarkably prolonged barrage of EPSCs.
403 Finally, 21 of the recorded PG cells, that either had an incomplete characterization
404 (n=17) or functional properties that did not fit in any of the 4 previously defined
405 subgroups (n=4), were not classified. 17 of these cells responded to the photo
406 stimulation with an IPSC.
407
408 **Diversity of basal forebrain afference**
409 Our data so far indicate that the time course of the basal forebrain synaptic inputs
410 depends on the PG cell subtype they target. To start gaining insight into whether these
411 distinct postsynaptic PG neurons are contacted by different presynaptic fibers, we
412 compared the short-term plasticity at these synapses. We applied a train of 5 blue light
413 pulses at 20 Hz. This photo stimulation evoked IPSCs that depressed at different
414 degrees in the three subclasses of type 2 PG cells as quantified by the paired-pulse
415 ratio of the second IPSC amplitude relative to the first (Kruskal-Wallis test, H=11.19,
416 p=0.0037)(Figure 7). In particular, the paired-pulse depression in CR-like PG cells
417 (0.73±0.13, n=11) was less pronounced than in CB-like PG cells (0.46±0.16, n=7,

418 p=0.0012, Wilcoxon test) and than in PG cells with long-lasting ON-evoked responses
419 (0.56±0.16, n=8, p=0.020, Wilcoxon test). The paired-pulse ratio was not different in
420 these two last groups (p=0.28, Wilcoxon test) but failures of transmission were
421 frequent in CB-like PG cells (seen in 5/7 cells, Figure 7B) whereas they were never
422 observed in PG cells with long-lasting ON-evoked responses. Together, these data
423 provide evidence that basal forebrain inputs may be mediated by specific afferent
424 fibers on each subclass of olfactory bulb PG cells.
425
426 **Discussion**
427 Most efforts in understanding the function of inhibition in the olfactory bulb have
428 focused on the local activation mechanisms of the diverse interneuron populations and
429 on the impact of their activity in shaping the olfactory bulb output. In comparison,
430 GABAergic circuits that control the activity of olfactory bulb interneurons have
431 received little attention. We show here that long-range GABAergic projections from
432 the basal forebrain make prominent and specific connections on most classes of
433 interneurons in the olfactory bulb with a previously unsuspected level of synaptic
434 specificity. These data provide additional criteria for PG cells classification and
435 emphasize that each PG cell subtype belongs to a specific synaptic circuit, an important
436 step towards understanding the functional implications of their diversity. They also
437 reinforce the idea that the basal forebrain is a major modulator of olfactory bulb
438 circuits whose influence is still partially understood.
439
440 **Basal forebrain projections to the olfactory bulb**
441 The basal forebrain contains several nuclei without clear delineations that
442 innervate the cerebral cortex, limbic areas, hippocampus, thalamic structures and the
443 olfactory bulb with cholinergic and GABAergic projections. Centrifugal projections to
444 the olfactory bulb originate principally from the HDB and MCPO. Cholinergic axons are
445 found essentially in the glomerular layer and in the internal plexiform layer of the bulb
446 and, moderately, in the granule cell layer (Macrides *et al.*, 1981; Zaborszky *et al.*, 1986;
447 Salcedo *et al.*, 2011; Case *et al.*, 2017; Hamamoto *et al.*, 2017). GABAergic projections
448 are even more massive and innervate all layers of the bulb (Zaborszky *et al.*, 1986;
449 Gracia-Llanes *et al.*, 2010; Niedworok *et al.*, 2012; Nunez-Parra *et al.*, 2013).

450 Cholinergic and GABAergic neurons are not clearly segregated in the basal forebrain
451 (Zaborszky *et al.*, 1986), interact between each other (Yang *et al.*, 2014) and nearly all
452 cholinergic neurons express the molecular machinery to co-transmit GABA (Saunders
453 *et al.*, 2015). These two centrifugal pathways are thus intimately coupled and attempts
454 to evaluate their influence independently have to be interpreted with caution.
455 Nevertheless, several reports demonstrate that ACh modulates diverse bulbar neurons
456 at different timescales and via multiple pre- and postsynaptic muscarinic and nicotinic
457 receptors (Castillo *et al.*, 1999; Ghatpande & Gelperin, 2009; Devore *et al.*, 2014; Liu *et*
458 *al.*, 2015; Smith *et al.*, 2015). Optogenetic manipulation of basal forebrain cholinergic
459 neurons modulates odor detection, discrimination and olfactory learning (Ma & Luo,
460 2012; Rothermel *et al.*, 2014). Our results indicate that basal forebrain GABAergic
461 neurons also have multiple targets in the bulb. Not surprisingly, pharmacological
462 inactivation of HDB/MCPO GABAergic neurons using a DREADD/CNO paradigm impairs
463 olfactory sensitivity and odor discrimination (Nunez-Parra *et al.*, 2013). The basal
464 forebrain therefore stands as a major modulator of olfactory bulb circuits but
465 understanding its global impact on olfactory bulb processing may first require a careful
466 investigation of its action on each targeted neuronal population.
467
468 **GABAergic synaptic connections discriminate different classes of PG cells**
469 We closely examined the GABAergic inputs of olfactory bulb PG cells. The results
470 demonstrate that GABAergic connections are an additional criterion that helps
471 classifying diverse PG cell subtypes. First, type 1 and type 2 PG cells can be
472 distinguished on the basis of their inhibitory input. Basal forebrain fibers contact
473 different subtypes of type 2 PG cells but not type 1 PG cells. Moreover, type 2 PG cells
474 have little synaptic interactions with other PG cells whereas type 1 PG cells do.
475 Previous studies revealed that GABAergic lateral interactions between PG cells
476 projecting within the same glomerulus are mediated, at least in part, by GABA spillover
477 (Smith & Jahr, 2002; Murphy *et al.*, 2005). Our results further suggest that more
478 conventional PG-PG cells synaptic interactions may be restricted to type 1 PG cells.
479 Second, we show that basal forebrain axons produce IPSCs with distinct time
480 courses and short term plasticities in three subgroups of type 2 PG cells that also differ
481 on the basis of their ON-evoked excitatory response and firing properties. IPSCs with

482 diverse durations likely reflect different subunit compositions of postsynaptic $GABA_A$
483 receptors. For instance, a subpopulation of PG cells that does not overlap with CB-, CR-
484 and TH-expressing cells selectively expresses the alpha5 subunit of the $GABA_A$ receptor
485 (Panzanelli *et al.*, 2007). Expression of this subunit correlates in some neurons with
486 slow IPSCs (Pangratz-Fuehrer *et al.*, 2016) suggesting that the alpha5 subunit may be a
487 molecular marker of the type 2 PG cells with regular firing and a long-lasting ON-
488 evoked excitatory response.

489 Postsynaptic $GABA_A$ receptors with different kinetics contribute in shaping short
490 term depression. However, our analysis of paired pulse ratio and failure rate suggest
491 that the different degrees at which basal forebrain IPSCs depressed in PG cells also
492 reflect presynaptic diversity. Thus, distinct subsets of chemically-defined basal
493 forebrain GABAergic neurons may control specific PG cell subclasses. Consistent with
494 this high level of centrifugal afferent selectivity, a recent report demonstrates that a
495 specific subset of GABA/ACh basal forebrain neurons preferentially projects in the
496 internal plexiform layer of the olfactory bulb where it selectively connects with one
497 specific subtype of dSA cells (Case *et al.*, 2017). Thus, addressing the synaptic
498 complexity of basal forebrain afferents in the glomerular layer of the olfactory bulb
499 may necessitate the use of transgenic mice allowing the manipulation of selective
500 genetically-identified population of neurons.

501

502 **Are there other classes of PG cells?**

503 We have defined four subclasses of PG cells based on functional parameters.
504 However, we limited our characterization to a subset of electrophysiological properties
505 that, in our recording conditions, could be unambiguously established. A full
506 characterization that correlates membrane and synaptic properties with morphological
507 and molecular features would most likely define additional subclasses of PG cells. For
508 instance, type 2 PG cells with short-lasting ON-evoked excitatory responses have
509 heterogeneous firing patterns and include CB-expressing and CB-lacking PG cells (Najac
510 *et al.*, 2015). In addition, some TH(+) juxtaglomerular neurons may constitute a
511 subclass of PG cells. These GABAergic/dopaminergic neurons constitute 20% of the
512 juxtaglomerular GABAergic cells (Panzanelli *et al.*, 2007; Parrish-Aungst *et al.*, 2007).
513 They are often collectively called superficial SA cells although only a small fraction of

514 them corresponds to the classical definition of superficial SA cells i.e. large TH(+) cells
515 with an axon and dendrites that widely ramify in the glomerular layer (Kosaka &
516 Kosaka, 2008; Kiyokage *et al.*, 2010; Galliano *et al.*, 2018). The majority though is
517 anaxonic and resembles the classical PG cells, with a small cell body and processes that
518 locally ramify, sometime within a single glomerulus (Kosaka & Kosaka, 2008; Galliano
519 *et al.*, 2018). We cannot exclude that small TH(+) cells have been included in our
520 analysis but they would constitute at most 1 out of 5 of our randomly recorded PG
521 cells. Moreover, their electrophysiological properties do not match well with any of the
522 four subclasses we defined. Small TH(+) juxtaglomerular cells fire spikes in a regular
523 manner but at low rate (Pignatelli *et al.*, 2005; Puopolo *et al.*, 2005; Galliano *et al.*,
524 2018) and a majority responds to the ON stimulation with a short polysynaptic
525 response (Kiyokage et al., 2010). Thus, our study does not address whether TH-
526 expressing juxtaglomerular neurons also receive basal forebrain inputs and future
527 experiments done in genetically identified TH(+) PG cells are needed to address this
528 important question.
529
530 **Role of basal forebrain GABAergic afferents in olfactory bulb odor processing**
531 We show the connections of basal forebrain GABA fibers with PG and granule cells
532 that, together, constitute the main populations of interneurons directly regulating the
533 activity of olfactory bulb output neurons. Deep SA cells also provide inhibitory input on
534 PG and granule cells (Eyre *et al.*, 2008; Burton *et al.*, 2017) and are themselves
535 modulated by basal forebrain inputs. This diversity of olfactory bulb interneurons
536 under the control of basal forebrain fibers makes it challenging to predict the global
537 functional implications of this GABAergic innervation on the olfactory bulb output. In
538 the simplest way, inhibition of olfactory bulb interneurons may induce a disinhibition
539 of mitral and tufted cells and thus facilitate the olfactory bulb output. However, GABA
540 may be excitatory on some PG cells (Parsa *et al.*, 2015). Moreover, co-transmission of
541 GABA and ACh on, at least, some interneurons (Case *et al.*, 2017), also complicates this
542 view. Moreover, as olfactory bulb processing is fundamentally rhythmic and tightly
543 coupled to respiration, the physiological impact of basal forebrain centrifugal inputs
544 may depend on their temporal dynamics along a respiration cycle. A synchronized
545 activity of these centrifugal afferents may reset the activity of olfactory bulb

interneurons before a new respiration cycle. But how synchronized are they? Recent data indicate that some non-cholinergic neurons in the HDB have their activity correlated with attention whereas the activity of cholinergic neurons is correlated with primary reinforcers and outcome expectations (Hangya *et al.*, 2015). Centrifugal inputs from the basal forebrain could therefore contextually modulate the olfactory bulb activity as a function of the internal state.

Interestingly, basal forebrain GABAergic fibers and axonal feedback from the olfactory cortex target the same populations of interneurons in the bulb. Thus, axons from pyramidal cells of the piriform cortex or the anterior olfactory nucleus directly excite olfactory bulb interneurons and facilitate mitral cell inhibition (Boyd *et al.*, 2012; Markopoulos *et al.*, 2012), i.e. the exact opposite of what HDB GABAergic fibers might do. Pyramidal cells of the olfactory cortex innervate HDB neurons as well (Paolini & McKenzie, 1997; Linster & Hasselmo, 2000) (Do *et al.*, 2016). Centrifugal afferents from the basal forebrain could have complex dynamics, similar as cortical feedback that exerts spatially diffuse, temporally complex and non-uniform actions on olfactory bulb interneurons in response to odors (Boyd *et al.*, 2015; Otazu *et al.*, 2015). Thus, the net impact of cortical feedback and basal forebrain fiber inputs on olfactory bulb interneurons, balancing or opposite actions, may depend on their relative timing in different behavioral context.

Acknowledgements

This work was supported by the Centre National pour la Recherche Scientifique, the Université de Strasbourg and the Agence Nationale pour la Recherche (Grant ANR-12-JSV4-006-01). ASD was funded by a fellowship from the Ministère de la Recherche and by a fellowship from the Fonds Paul Mandel pour les Recherches en Neuroscience. We thank Ipek Yalcin (Institut des Neurosciences Cellulaires et Intégratives, Strasbourg) and Claire Gaveriaux-Ruff (Institut de Génétique et de Biologie Moléculaire et Cellulaire, Strasbourg) for the kind gift of the dlx5/6-Cre mice and Thomas Knöpfel (Imperial College, London) for the kind gift of the Kv3.1-EYFP mice. We thank Sophie Reibel-Foisset and the animal facility Chronobiotron (UMS 3415 Centre National pour la Recherche Scientifique and Université de Strasbourg), the Plateforme Imagerie In Vitro-Neuropôle-Strasbourg, and Aline Huber for their technical assistance. We thank Jean Christophe Cassel (Laboratoire de Neurosciences Cognitives et Adaptatives, Strasbourg) Nuria Benito, Philippe Isope, Matilde Cordero-Erausquin, Bernard Poulain, and members of the lab for their constructive comments throughout the project.

582 **References**

583 Abraham NM, Egger V, Shimshek DR, Renden R, Fukunaga I, Sprengel R, Seeburg PH,
584 Klugmann M, Margrie TW, Schaefer AT & Kuner T. (2010). Synaptic inhibition in the
585 olfactory bulb accelerates odor discrimination in mice. *Neuron* **65,** 399-411.
586
587 Benito N, Gaborieau E, Sanz Diez A, Kosar S, Foucault L, Raineteau O & De Saint Jan D.
588 (2018). A pool of postnatally-generated interneurons persists in an immature stage in
589 the olfactory bulb. *J Neurosci*.
590
591 Boyd AM, Kato HK, Komiyama T & Isaacson JS. (2015). Broadcasting of cortical activity
592 to the olfactory bulb. *Cell Rep* **10,** 1032-1039.
593
594 Boyd AM, Sturgill JF, Poo C & Isaacson JS. (2012). Cortical feedback control of olfactory
595 bulb circuits. *Neuron* **76,** 1161-1174.
596
597 Burton SD, LaRocca G, Liu A, Cheetham CE & Urban NN. (2017). Olfactory Bulb Deep
598 Short-Axon Cells Mediate Widespread Inhibition of Tufted Cell Apical Dendrites. *J*
599 *Neurosci* **37,** 1117-1138.
600
601 Case DT, Burton SD, Gedeon JY, Williams SG, Urban NN & Seal RP. (2017). Layer- and
602 cell type-selective co-transmission by a basal forebrain cholinergic projection to the
603 olfactory bulb. *Nat Commun* **8,** 652.
604
605 Castillo PE, Carleton A, Vincent JD & Lledo PM. (1999). Multiple and opposing roles of
606 cholinergic transmission in the main olfactory bulb. *J Neurosci* **19,** 9180-9191.
607
608 Devore S, de Almeida L & Linster C. (2014). Distinct roles of bulbar muscarinic and
609 nicotinic receptors in olfactory discrimination learning. *J Neurosci* **34,** 11244-11260.
610
611 Do JP, Xu M, Lee SH, Chang WC, Zhang S, Chung S, Yung TJ, Fan JL, Miyamichi K, Luo L &
612 Dan Y. (2016). Cell type-specific long-range connections of basal forebrain circuit. *Elife*
613 **5**.
614
615 Economo MN, Hansen KR & Wachowiak M. (2016). Control of Mitral/Tufted Cell
616 Output by Selective Inhibition among Olfactory Bulb Glomeruli. *Neuron* **91,** 397-411.
617
618 Eyre MD, Antal M & Nusser Z. (2008). Distinct deep short-axon cell subtypes of the
619 main olfactory bulb provide novel intrabulbar and extrabulbar GABAergic connections.
620 *J Neurosci* **28,** 8217-8229.
621
622 Fogli Iseppe A, Pignatelli A & Belluzzi O. (2016). Calretinin-Periglomerular Interneurons
623 in Mice Olfactory Bulb: Cells of Few Words. *Front Cell Neurosci* **10,** 231.
624
625 Fukunaga I, Herb JT, Kollo M, Boyden ES & Schaefer AT. (2014). Independent control of
626 gamma and theta activity by distinct interneuron networks in the olfactory bulb. *Nat*
627 *Neurosci* **17,** 1208-1216.
628

629 Galliano E, Franzoni E, Breton M, Chand AN, Byrne DJ, Murthy VN & Grubb MS. (2018).
630 Embryonic and postnatal neurogenesis produce functionally distinct subclasses of
631 dopaminergic neuron. *Elife* **7**.
632
633 Geramita M & Urban NN. (2017). Differences in Glomerular-Layer-Mediated
634 Feedforward Inhibition onto Mitral and Tufted Cells Lead to Distinct Modes of Intensity
635 Coding. *J Neurosci* **37,** 1428-1438.
636
637 Ghatpande AS & Gelperin A. (2009). Presynaptic muscarinic receptors enhance
638 glutamate release at the mitral/tufted to granule cell dendrodendritic synapse in the
639 rat main olfactory bulb. *J Neurophysiol* **101,** 2052-2061.
640
641 Gracia-Llanes FJ, Crespo C, Blasco-Ibanez JM, Nacher J, Varea E, Rovira-Esteban L &
642 Martinez-Guijarro FJ. (2010). GABAergic basal forebrain afferents innervate selectively
643 GABAergic targets in the main olfactory bulb. *Neuroscience* **170,** 913-922.
644
645 Gschwend O, Abraham NM, Lagier S, Begnaud F, Rodriguez I & Carleton A. (2015).
646 Neuronal pattern separation in the olfactory bulb improves odor discrimination
647 learning. *Nat Neurosci* **18,** 1474-1482.
648
649 Hamamoto M, Kiyokage E, Sohn J, Hioki H, Harada T & Toida K. (2017). Structural basis
650 for cholinergic regulation of neural circuits in the mouse olfactory bulb. *J Comp Neurol*
651 **525,** 574-591.
652
653 Hangya B, Ranade SP, Lorenc M & Kepecs A. (2015). Central Cholinergic Neurons Are
654 Rapidly Recruited by Reinforcement Feedback. *Cell* **162,** 1155-1168.
655
656 Kiyokage E, Pan YZ, Shao Z, Kobayashi K, Szabo G, Yanagawa Y, Obata K, Okano H,
657 Toida K, Puche AC & Shipley MT. (2010). Molecular identity of periglomerular and short
658 axon cells. *J Neurosci* **30,** 1185-1196.
659
660 Kosaka K & Kosaka T. (2007). Chemical properties of type 1 and type 2 periglomerular
661 cells in the mouse olfactory bulb are different from those in the rat olfactory bulb.
662 *Brain Res* **1167,** 42-55.
663
664 Kosaka T & Kosaka K. (2008). Tyrosine hydroxylase-positive GABAergic juxtaglomerular
665 neurons are the main source of the interglomerular connections in the mouse main
666 olfactory bulb. *Neurosci Res* **60,** 349-354.
667
668 Kosaka T & Kosaka K. (2011). "Interneurons" in the olfactory bulb revisited. *Neurosci*
669 *Res* **69,** 93-99.
670
671 Lepousez G & Lledo PM. (2013). Odor discrimination requires proper olfactory fast
672 oscillations in awake mice. *Neuron* **80,** 1010-1024.
673

674 Linster C & Hasselmo ME. (2000). Neural activity in the horizontal limb of the diagonal
675 band of broca can be modulated by electrical stimulation of the olfactory bulb and
676 cortex in rats. *Neurosci Lett* **282,** 157-160.
677
678 Liu S, Plachez C, Shao Z, Puche A & Shipley MT. (2013). Olfactory bulb short axon cell
679 release of GABA and dopamine produces a temporally biphasic inhibition-excitation
680 response in external tufted cells. *J Neurosci* **33,** 2916-2926.
681
682 Liu S, Shao Z, Puche A, Wachowiak M, Rothermel M & Shipley MT. (2015). Muscarinic
683 receptors modulate dendrodendritic inhibitory synapses to sculpt glomerular output. *J*
684 *Neurosci* **35,** 5680-5692.
685
686 Ma M & Luo M. (2012). Optogenetic activation of basal forebrain cholinergic neurons
687 modulates neuronal excitability and sensory responses in the main olfactory bulb. *J*
688 *Neurosci* **32,** 10105-10116.
689
690 Macrides F, Davis BJ, Youngs WM, Nadi NS & Margolis FL. (1981). Cholinergic and
691 catecholaminergic afferents to the olfactory bulb in the hamster: a neuroanatomical,
692 biochemical, and histochemical investigation. *J Comp Neurol* **203,** 495-514.
693
694 Markopoulos F, Rokni D, Gire DH & Murthy VN. (2012). Functional properties of
695 cortical feedback projections to the olfactory bulb. *Neuron* **76,** 1175-1188.
696
697 McQuiston AR & Katz LC. (2001). Electrophysiology of interneurons in the glomerular
698 layer of the rat olfactory bulb. *J Neurophysiol* **86,** 1899-1907.
699
700 Metzger F, Repunte-Canonigo V, Matsushita S, Akemann W, Diez-Garcia J, Ho CS,
701 Iwasato T, Grandes P, Itohara S, Joho RH & Knopfel T. (2002). Transgenic mice
702 expressing a pH and Cl- sensing yellow-fluorescent protein under the control of a
703 potassium channel promoter. *Eur J Neurosci* **15,** 40-50.
704
705 Monory K, Massa F, Egertova M, Eder M, Blaudzun H, Westenbroek R, Kelsch W, Jacob
706 W, Marsch R, Ekker M, Long J, Rubenstein JL, Goebbels S, Nave KA, During M,
707 Klugmann M, Wolfel B, Dodt HU, Zieglgansberger W, Wotjak CT, Mackie K, Elphick MR,
708 Marsicano G & Lutz B. (2006). The endocannabinoid system controls key epileptogenic
709 circuits in the hippocampus. *Neuron* **51,** 455-466.
710
711 Murphy GJ, Darcy DP & Isaacson JS. (2005). Intraglomerular inhibition: signaling
712 mechanisms of an olfactory microcircuit. *Nat Neurosci* **8,** 354-364.
713
714 Najac M, Sanz Diez A, Kumar A, Benito N, Charpak S & De Saint Jan D. (2015).
715 Intraglomerular lateral inhibition promotes spike timing variability in principal neurons
716 of the olfactory bulb. *J Neurosci* **35,** 4319-4331.
717
718 Niedworok CJ, Schwarz I, Ledderose J, Giese G, Conzelmann KK & Schwarz MK. (2012).
719 Charting monosynaptic connectivity maps by two-color light-sheet fluorescence
720 microscopy. *Cell Rep* **2,** 1375-1386.

721
722 Nunez-Parra A, Maurer RK, Krahe K, Smith RS & Araneda RC. (2013). Disruption of
723 centrifugal inhibition to olfactory bulb granule cells impairs olfactory discrimination.
724 *Proc Natl Acad Sci U S A* **110,** 14777-14782.
725
726 Otazu GH, Chae H, Davis MB & Albeanu DF. (2015). Cortical Feedback Decorrelates
727 Olfactory Bulb Output in Awake Mice. *Neuron* **86,** 1461-1477.
728
729 Pangratz-Fuehrer S, Sieghart W, Rudolph U, Parada I & Huguenard JR. (2016). Early
730 postnatal switch in GABAA receptor alpha-subunits in the reticular thalamic nucleus. *J*
731 *Neurophysiol* **115,** 1183-1195.
732
733 Panzanelli P, Fritschy JM, Yanagawa Y, Obata K & Sassoe-Pognetto M. (2007).
734 GABAergic phenotype of periglomerular cells in the rodent olfactory bulb. *J Comp*
735 *Neurol* **502,** 990-1002.
736
737 Paolini AG & McKenzie JS. (1997). Intracellular recording of magnocellular preoptic
738 neuron responses to olfactory brain. *Neuroscience* **78,** 229-242.
739
740 Parrish-Aungst S, Shipley MT, Erdelyi F, Szabo G & Puche AC. (2007). Quantitative
741 analysis of neuronal diversity in the mouse olfactory bulb. *J Comp Neurol* **501,** 825-836.
742
743 Parsa PV, D'Souza RD & Vijayaraghavan S. (2015). Signaling between periglomerular
744 cells reveals a bimodal role for GABA in modulating glomerular microcircuitry in the
745 olfactory bulb. *Proc Natl Acad Sci U S A* **112,** 9478-9483.
746
747 Pignatelli A, Kobayashi K, Okano H & Belluzzi O. (2005). Functional properties of
748 dopaminergic neurones in the mouse olfactory bulb. *J Physiol* **564,** 501-514.
749
750 Puopolo M, Bean BP & Raviola E. (2005). Spontaneous activity of isolated dopaminergic
751 periglomerular cells of the main olfactory bulb. *J Neurophysiol* **94,** 3618-3627.
752
753 Rothermel M, Carey RM, Puche A, Shipley MT & Wachowiak M. (2014). Cholinergic
754 inputs from Basal forebrain add an excitatory bias to odor coding in the olfactory bulb.
755 *J Neurosci* **34,** 4654-4664.
756
757 Salcedo E, Tran T, Ly X, Lopez R, Barbica C, Restrepo D & Vijayaraghavan S. (2011).
758 Activity-dependent changes in cholinergic innervation of the mouse olfactory bulb.
759 *PLoS One* **6,** e25441.
760
761 Saunders A, Granger AJ & Sabatini BL. (2015). Corelease of acetylcholine and GABA
762 from cholinergic forebrain neurons. *Elife* **4**.
763
764 Shao Z, Puche AC, Kiyokage E, Szabo G & Shipley MT. (2009). Two GABAergic
765 intraglomerular circuits differentially regulate tonic and phasic presynaptic inhibition
766 of olfactory nerve terminals. *J Neurophysiol* **101,** 1988-2001.
767

768 Smith RS, Hu R, DeSouza A, Eberly CL, Krahe K, Chan W & Araneda RC. (2015).
769 Differential Muscarinic Modulation in the Olfactory Bulb. *J Neurosci* **35,** 10773-10785.
770
771 Smith TC & Jahr CE. (2002). Self-inhibition of olfactory bulb neurons. *Nat Neurosci* **5,**
772 760-766.
773
774 Whitesell JD, Sorensen KA, Jarvie BC, Hentges ST & Schoppa NE. (2013).
775 Interglomerular lateral inhibition targeted on external tufted cells in the olfactory bulb.
776 *J Neurosci* **33,** 1552-1563.
777
778 Whitman MC & Greer CA. (2007). Adult-generated neurons exhibit diverse
779 developmental fates. *Dev Neurobiol* **67,** 1079-1093.
780
781 Yang C, McKenna JT, Zant JC, Winston S, Basheer R & Brown RE. (2014). Cholinergic
782 neurons excite cortically projecting basal forebrain GABAergic neurons. *J Neurosci* **34,**
783 2832-2844.
784
785 Zaborszky L, Buhl DL, Pobalashingham S, Bjaalie JG & Nadasdy Z. (2005). Three-
786 dimensional chemoarchitecture of the basal forebrain: spatially specific association of
787 cholinergic and calcium binding protein-containing neurons. *Neuroscience* **136,** 697-
788 713.
789
790 Zaborszky L, Carlsen J, Brashear HR & Heimer L. (1986). Cholinergic and GABAergic
791 afferents to the olfactory bulb in the rat with special emphasis on the projection
792 neurons in the nucleus of the horizontal limb of the diagonal band. *J Comp Neurol* **243,**
793 488-509.
794
795

796 **Competing interests** : The authors declare no competing financial interests.

797 **Figures and legends**

798

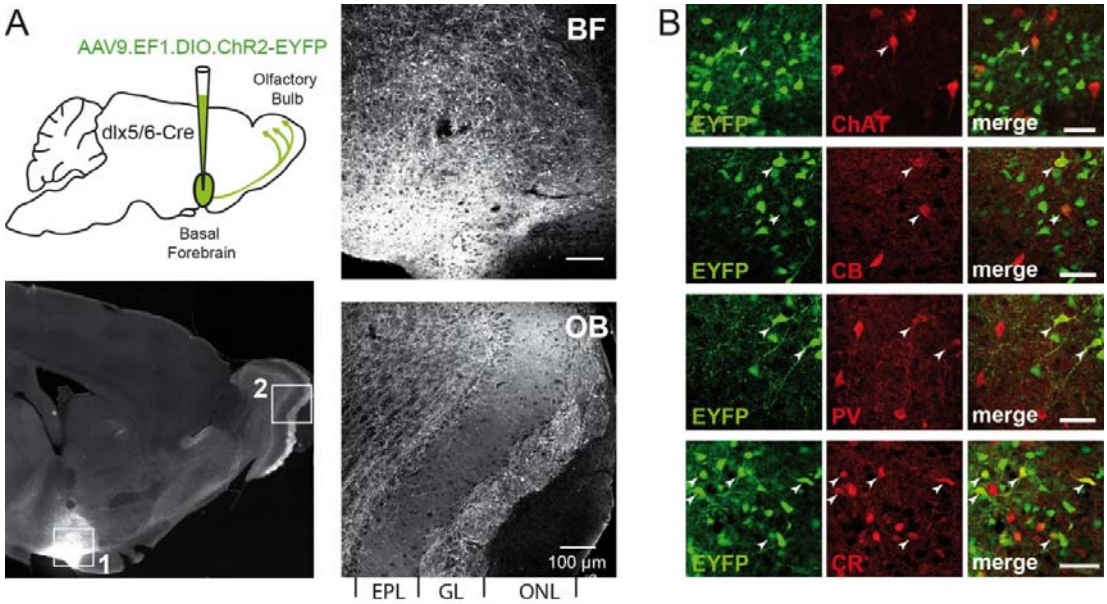

799

800

801 **Figure 1: Conditional expression of ChR2 in various GABAergic neurons of the basal**
802 **forebrain. A,** Stereotaxic injection of a viral construct in the basal forebrain of dlx5/6-
803 Cre mice was used for conditional expression of ChR2-EYFP in GABAergic neurons of
804 the basal forebrain. Bottom left, sagittal section of a brain 4 weeks after the injection.
805 The site of injection (BF, boxed area 1) and the olfactory bulb (OB, boxed area 2) are
806 enlarged in the two other pictures. ONL: olfactory nerve layer, GL: glomerular layer,
807 EPL: external plexiform layer. **B,** EYFP expression in the basal forebrain 4 weeks after
808 injection of the same viral construct encoding cytosolic EYFP. Co-staining of EYFP
809 (green) together with ChAT, CB, PV or CR (red). Some neurons (arrowheads), but not
810 all, co-express the two markers. Scale bars 50 µm.

811

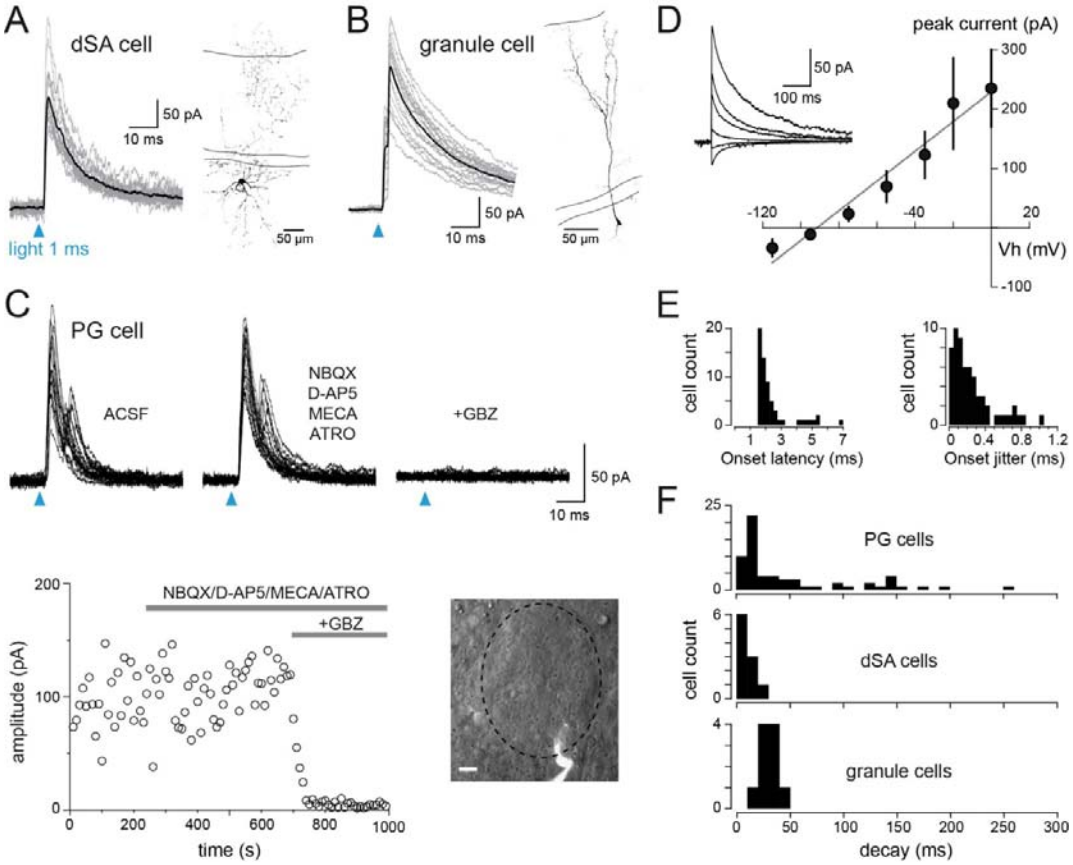

<u>Figure 2</u>. Synaptic connections of basal forebrain axons with various inhibitory interneurons of the olfactory bulb. A, Light-evoked consecutive ISPCs evoked in a deep SA cell recorded at Vh=-35 mV in the presence of AMPA and NMDA receptor blockers (10 µM NBQX + 50 µM D-AP5). The black trace is the average response. Light stimulation (1 ms) at blue arrow. The morphology of this neurobiotin-filled cell is shown. Solid lines delimit the glomerular layer (top) and the mitral cell layer (bottom). **B,** Same in a granule cell recorded at Vh=0 mV. **C,** Light-evoked IPSCs elicited in a PG cell (Vh=0mV) in control condition, in the presence of NBQX (10 µM), D-AP5 (50 µM), mecamylamine (MECA, 20 µM) and atropine (ATRO, 10 µM) and after the addition of gabazine (5 µM, GBZ) to the cocktail. Several traces are superimposed for each condition. The graph shows the amplitude of consecutive responses in these different conditions. The image on the right is a snapshot of this PG cell during the recording, superimposed on the DIC image of the glomerulus delimited by a dashed line. Scale bar 10 µm. **D,** Average current-voltage relationship of the light-evoked IPSC in PG cells (n=12 cells, each plot is an average±sem). Inset, IPSCs from a representative PG cell

829 recorded at different holding potentials. **E,** Distribution histograms of the onset latency
830 (left) and onset jitter (right) of light-evoked IPSCs recorded in PG cells. **F,** Decay time
831 constants distribution of light-evoked IPSCs recorded in PG, dSA and granule cells. PG
832 and granule cells were recorded at Vh=0mV, dSA cells at Vh comprised between -35
833 mV and -15 mV.
834
835
836

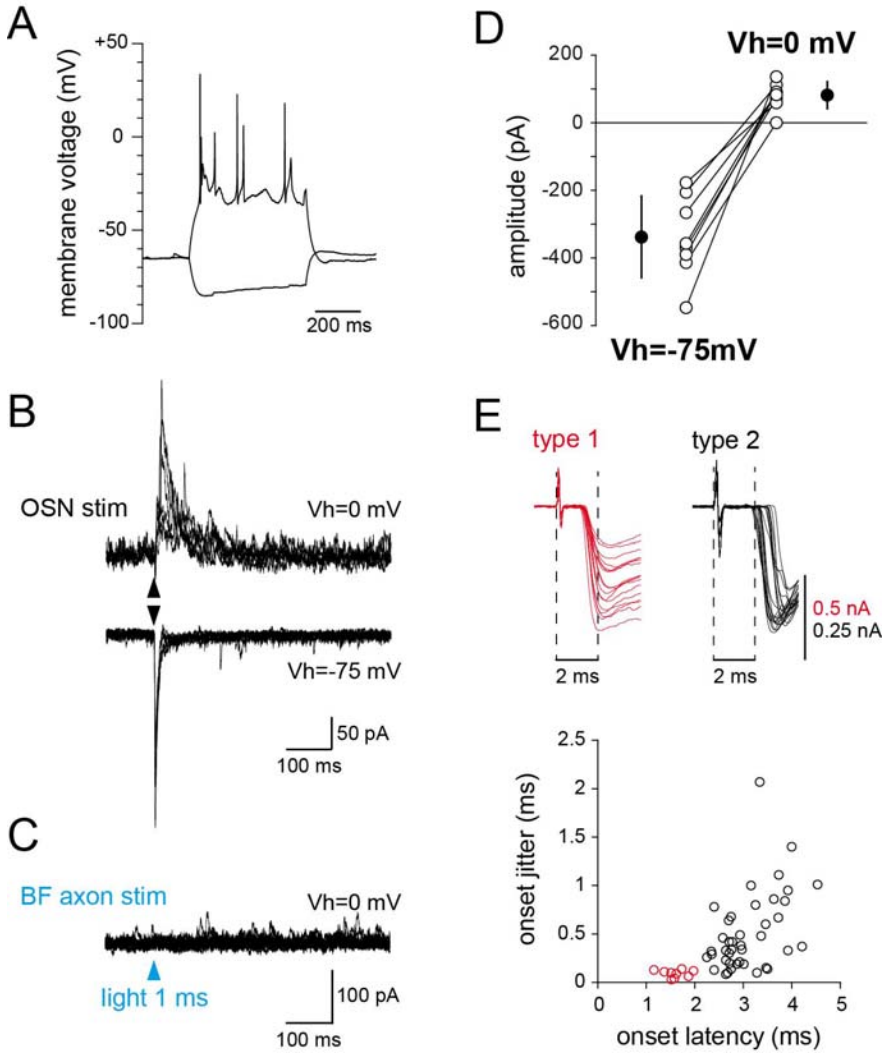

<u>Figure 3</u>: Type 1 PG cells are not contacted by basal forebrain projections but are inhibited by other PG cells. Membrane properties (**A**), ON-evoked synaptic responses (**B**) and responses to basal forebrain axons photo stimulation (**C**) of a type 1 PG cell recorded in a dlx5/6;ChR2-EYFP mouse. This cell responded to the stimulation of OSN axons with an inward fast monosynaptic EPSC at Vh=-75 mV and with outward plurisynaptic IPSCs at Vh=0 mV (**B**). In contrast, light stimulation of basal forebrain fibers did not evoke any response (**C**). Several traces are superimposed in each case. **D,** Summary plots for ON-evoked synaptic response amplitudes of all type 1 PG cells tested at two holding potentials. **E,** Classification of the recorded PG cells into type 1 and type 2 in dlx5/6;ChR2-EYFP mice. Top, early phase of ON-evoked EPSCs in a type 1

850 PG cell (red) and in a type 2 PG cell (black). The type 1 PG cell responded with a short
851 latency EPSC, starting <2ms after the beginning of the stimulation artifact and with
852 little onset variability between trials. In contrast, responses from the type 2 PG cell had
853 a delayed and more variable onset latency. The graph shows the onset latency vs.
854 onset jitter of ON-evoked responses in PG cells classified as type 1 PG cells (red circles)
855 and in PG cells classified as type 2 PG cells (black circles) in this study.
856

857

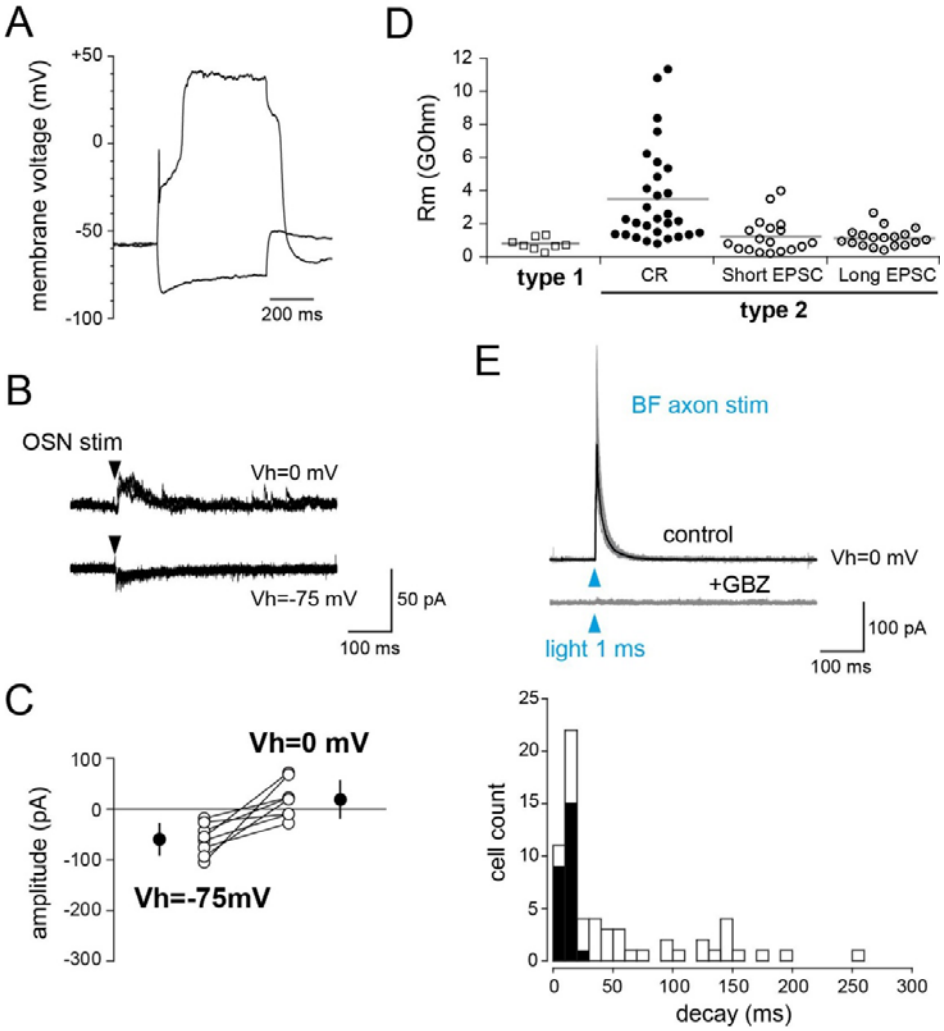

858

859

860 **<u>Figure 4</u>: CR-expressing type 2 PG cells receive fast basal forebrain GABAergic inputs.**
861 Membrane properties (**A**) and ON-evoked synaptic responses (**B**) of a typical CR-
862 expressing type 2 PG cell recorded in a dlx5/6;ChR2-EYFP mouse. This cell typically
863 responded to a suprathreshold depolarization with a single spikelet followed by a
864 passive membrane depolarization (**A**) and had small ON-evoked responses at Vh=-75
865 mV and at Vh=0 mV (**B**). **C**, summary plots for ON-evoked synaptic responses recorded
866 at Vh=-75 mV and at Vh=0 mV for cells classified as CR-expressing PG cells. **D**, cells
867 classified as CR-expressing type 2 PG cells also had larger electrical membrane
868 resistances compared to PG cells classified in the other groups (horizontal bars show
869 the averages, $p<0.001$ for comparison with each of the 3 other subgroups, Wilcoxon
870 test). **E,** light stimulation of basal forebrain fibers evoked large and fast GBZ-sensitive

871 IPSCs in CR-expressing PG cells. Traces are from the same cell as in A and B. The
872 average IPSC (black trace) is superimposed on several consecutive responses recorded
873 at Vh=0mV in ACSF. Bottom, distribution histogram of the decay time constants of
874 light-evoked IPSCs in cells classified as CR-expressing PG cells (black bars)
875 superimposed on the distribution histogram for all the recorded PG cells (white bars).
876

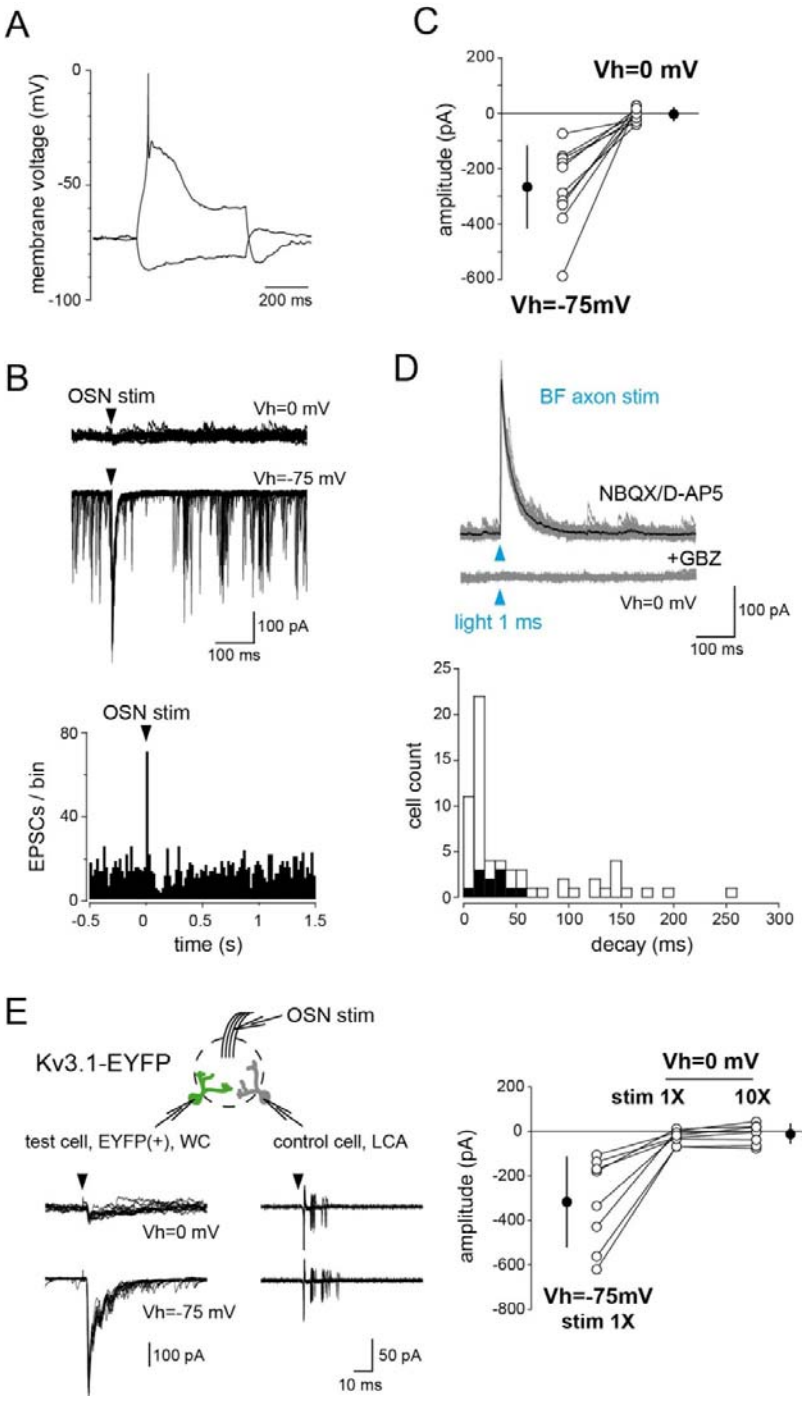

<u>Figure 5</u>: Type 2 PG cells with short ON-evoked excitatory response do not interact with other PG cells but receive inputs from the basal forebrain. Membrane properties (**A**) and ON-evoked synaptic responses (**B**) of a typical type 2 PG cell that responded to the stimulation of the OSN axons with a short burst of EPSCs in a dlx5/6;ChR2-EYFP mouse. The short ON-evoked excitatory response was the main criterion for classifying

884 PG cells in this subclass. **C**, Summary plots (right) for ON-evoked synaptic responses
885 recorded at Vh=-75 mV and at Vh=0 mV indicate that cells in this group also had no
886 ON-evoked IPSC. **D**, IPSCs evoked by a light stimulation of the basal forebrain fibers.
887 The average IPSC (black trace) is superimposed on several consecutive responses
888 recorded at Vh=0mV in the presence of NBQX and D-AP5. GBZ abolished the response.
889 Traces are from the same cell as in A and B. Bottom, distribution histogram of the
890 decay time constants of light-evoked IPSCs in PG cells classified in this subclass (black
891 bars) superimposed on the distribution histogram for all the recorded PG cells (white
892 bars). **E**, Paired recording of two PG cells projecting in the same glomerulus in the
893 Kv3.1-EYFP transgenic mouse. The "test" EYFP(+) PG cell was recorded in the whole-
894 cell configuration at Vh=0 mV to monitor IPSCs and at Vh=-75 mV to monitor EPSCs.
895 The "control" PG cell was recorded in the loose cell-attached configuration to monitor
896 its firing. OSNs were stimulated at an intensity inducing the firing of the control PG cell.
897 The summary graph on the right shows that OSN stimulations did not evoke any
898 outward IPSC in the test cell even when the stimulation was increased by a factor of
899 10.
900

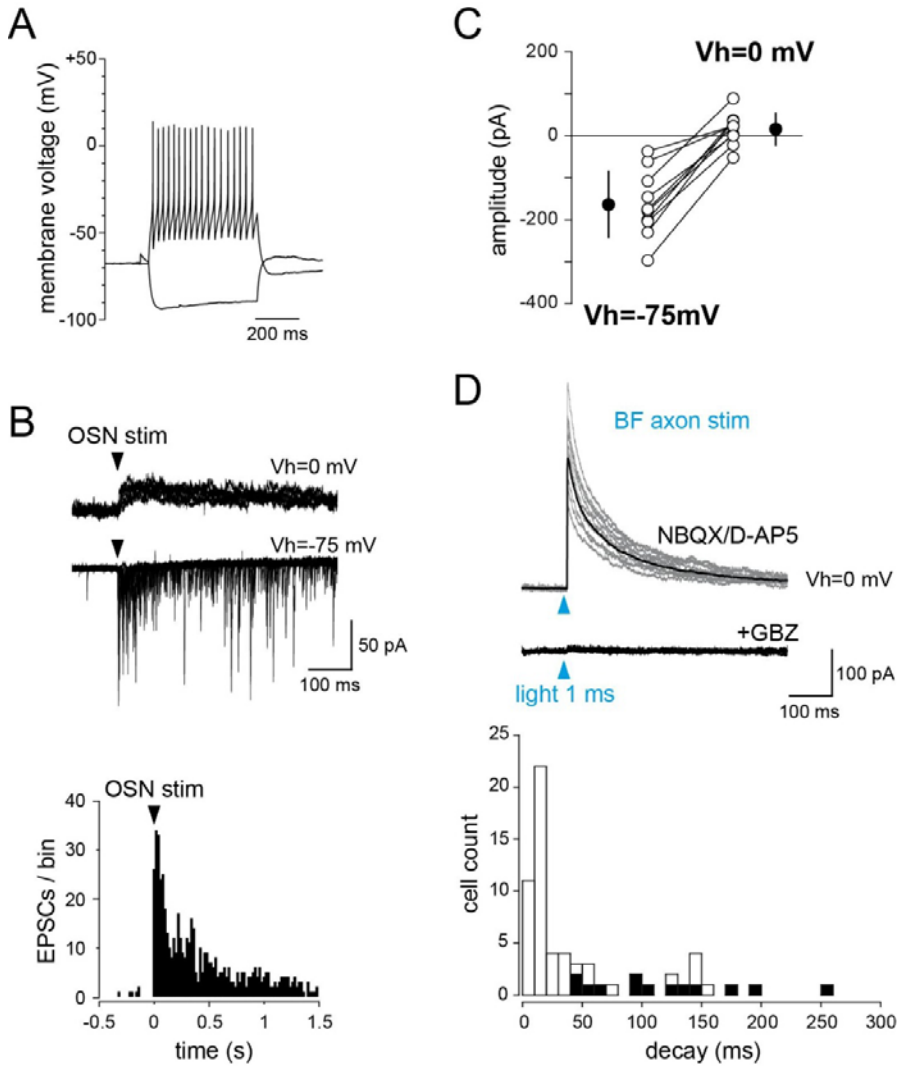

<u>Figure 6</u>: Type 2 PG cells with long-lasting ON-evoked excitatory response receive slow GABAergic inputs from the basal forebrain. Membrane properties (**A**) and ON-evoked synaptic responses of a typical type 2 PG cell that responded to the stimulation of the OSN axons with a long-lasting burst of EPSCs in a dlx5/6;ChR2-EYFP mouse. **A**, Like all the cells included in this group, this PG cell responded to a step depolarization with a regular firing. **B**, ON-evoked responses recorded at two holding potentials and PSTH of the excitatory response (bottom). **C**, Summary plots for ON-evoked synaptic responses recorded at Vh=-75 mV and at Vh=0 mV for cells included in this group. **D**, IPSCs evoked by a light stimulation of the basal forebrain fibers. The average IPSC (black trace) is superimposed on several consecutive responses recorded at Vh=0mV in the presence of NBQX and D-AP5. GBZ abolished the response. Same cell as in A and B.

914 Bottom, distribution histogram of the decay time constants of light-evoked IPSCs in PG
915 cells classified in this subclass (black bars) superimposed on the distribution histogram
916 for all the recorded PG cells (white bars). Cells included in this group had slow IPSCs.
917

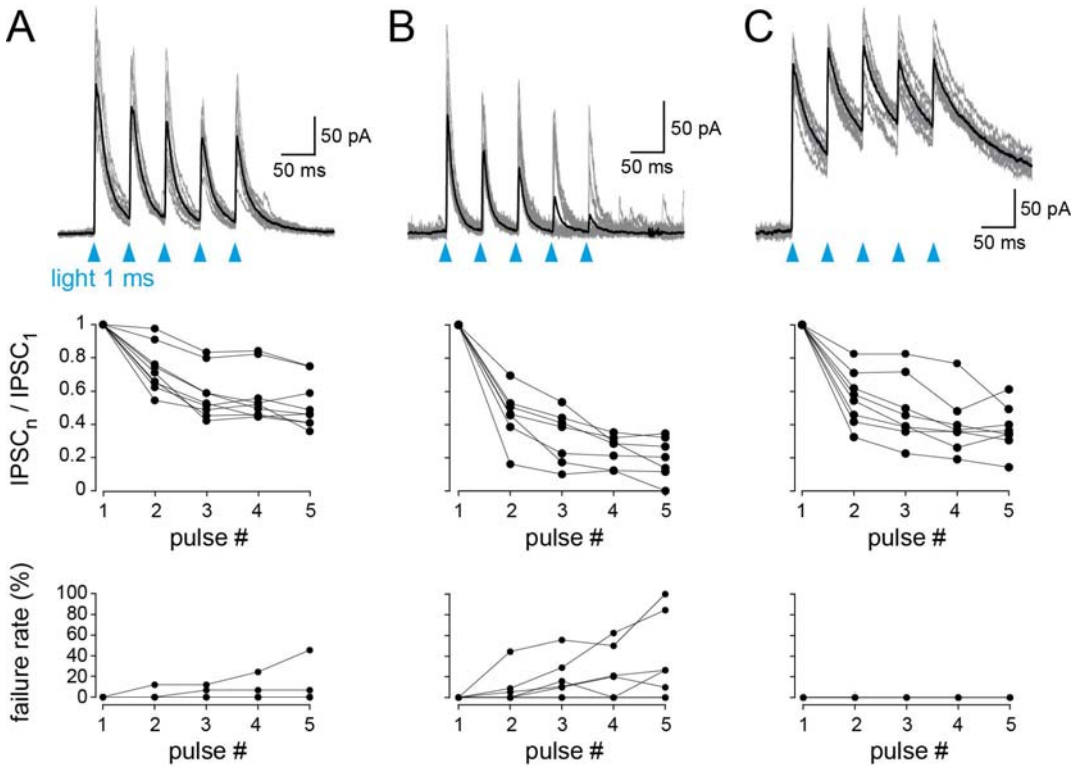

Figure 7 : Basal forebrain GABAergic inputs have different presynaptic properties depending on the postsynaptic PG cell subtype. A-C, Top row, light-evoked IPSCs in three PG cells representative of the three subclasses of type 2 PG cells recorded in dlx5/6;ChR2-EYFP mice (**A**: CR-expressing PG cells; **B**: PG cells with short ON-evoked excitatory responses and **C**: regularly firing PG cells with long-lasting ON-evoked responses). Each cell was stimulated with 5 flashes of light at 20 Hz. 10-12 consecutive responses are superimposed for each cell, the black trace is the average response. **Middle row,** amplitudes of the nth light-evoked IPSC relative to the normalized amplitude of the first IPSC recorded in PG cells classified in the 3 subgroups of the corresponding column. Lines connect plots from the same cells. **Bottom row**, failure rate for each of the five consecutive stimuli and for each cell over multiple trials. Failures were never observed in the third group.